

# Kinetic Arrest in Polyion-Induced Inhomogeneously-Charged Colloidal Particle Aggregation

D. Truzzolillo, F. Bordi, F. Sciortino, C. Cametti

*Dipartimento di Fisica, Università di Roma "La Sapienza"*

*Piazzale A. Moro 5, I-00185 - Rome (Italy) and INFM CRS-SOFT, Unita' di Roma 1*

(Dated: May 26, 2008)

Polymer chains adsorbed onto oppositely charged spherical colloidal particles can significantly modify the particle-particle interactions. For sufficient amounts of added polymers, the original electrostatic repulsion can even turn into an effective attraction and relatively large kinetically stable aggregates can form. The attractive interaction contribution between two oppositely particles arises from the *correlated* adsorption of polyions at the oppositely charged particle surfaces, resulting in a non-homogeneous surface charge distribution. Here, we investigate the aggregation kinetics of polyion-induced colloidal complexes through Monte Carlo simulation, in which the effect of charge anisotropy is taken into account by a DLVO-like intra-particle potential, as recently proposed by Velegol and Thwar [*D. Velegol and P.K. Thwar, Langmuir, 17, 2001*]. The results reveal that in the presence of a charge heterogeneity the aggregation process slows down due to the progressive increase of the potential barrier height upon clustering. Within this framework, the experimentally observed cluster phases in polyelectrolyte-liposomes solutions should be considered as a kinetic arrested state.

## 1. INTRODUCTION

The addition of oppositely charged polyions to a suspension of charged colloidal particles gives rise to an intriguing and partially unexpected phenomenology<sup>1,2</sup>, resulting in the formation of aggregates which play an important role in a wide range of implications<sup>3,4,5</sup>, from membrane biophysics and soft matter physics<sup>6,7,8</sup> to biotechnological processes, such as therapeutic delivery systems<sup>9</sup>.

These aggregates are governed by a delicate balance between attractive and repulsive interactions resulting in the appearance of an equilibrium (or a kinetically arrested) cluster phase, where single particles, stuck together by an electrostatic "glue" acting between oppositely charge domains, form reversible, relatively large, complexes. In this system, the short-range attraction contribution is promoted by the addition of "adsorbing" polyions which form a two-dimensional strongly correlated, short-range ordered, structure on the surface of the oppositely charged particle, contrarily to what happens for "non-adsorbing" polymers, where the attraction contribution is produced by the unbalanced osmotic pressure in the depletion regime.

In fact, correlated adsorption of polyion chains on the surface of oppositely charged particles induces two different phenomena: "charge inversion"<sup>1,2,6,7</sup> and "reentrant condensation"<sup>1,2,10</sup>. The first one occurs when a colloidal particle binds several oppositely charged multivalent ions (polyions), so that its effective charge inverts its sign. The second effect, concomitant to the charge inversion, consists in the formation of particle aggregates whose average size increases on increasing the polyion concentration, until it reaches a maximum (at the point of charge inversion), decreasing afterwards to the initial value.

This phenomenology has been investigated in a variety of different colloidal systems both for particles bear-

ing a negative charge (such as DOTAP liposomes) in the presence of anionic polyions<sup>1</sup> and for positively charged particles (such as hybrid niosomes) in the presence of cationic polyions<sup>11</sup>. The occurrence of a sharp reentrant condensation on increasing the adsorption of polyion on charged liposomes has been documented in a series of articles<sup>1,2,10</sup>. It has been shown that the size of the aggregates goes through a maximum and their overall charge inverts its sign in concomitance to the point of charge inversion, as briefly reviewed in Fig. 1 for some typical cationic or anionic colloidal particle systems. The formation of aggregates and, consequently, the stability of colloidal charged particles (solid particles or soft vesicles) is usually satisfactorily explained in the framework of Derjaguin-Landau-Verwey-Overbeek (DLVO) theory<sup>12</sup>, which accounts for electrostatic and van der Waals interactions between two approaching particles. In the traditional DLVO theory, the particle surface is assumed to be uniformly charged. In the case of polyion-correlated adsorption onto the surface of the particle, this assumption is no longer valid and the usual DLVO theory might not account for the effects arising from the surface charge heterogeneity. Indeed, the adsorption of the polymer generates an ordered charged structure, strongly dependent on the polyion size and on the valence and linear charge density<sup>6</sup>. Some experimental evidences of such a structure can be found in Refs.[13] and [14]. Transmission electron microscopy [TEM] measurements suggest the formation of a local "patchy charge distribution". In this respect, it is reasonable to expect that attractive interactions can arise when "counterion domains" on one particle align to a "counterion-free domains" on another approaching particle.

Recently, Velegol and Thwar<sup>15</sup> have developed an analytical model for the effective particle-particle potential  $\langle \Phi \rangle$  in the case of non-uniform charge distributions, based on the Derjaguin approximation and on an extension of the Hogg-Healy-Fuerstenau [HHF]<sup>16</sup> model for randomly

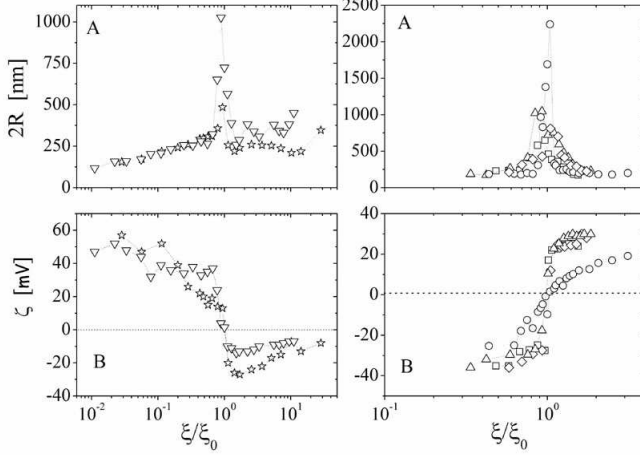


FIG. 1: Fig. 1 - A brief review of the experimental evidence showing a non-monotonic increase of the size of the polyion-induced charged particle aggregates, in the presence of oppositely charged polyions. Both positively and negatively charged particles are shown. Left panels: reentrant condensation (aggregate radius  $R$ ) (A) and charge inversion ( $\zeta$ -potential) (B) of positively charged liposomes, in the presence of negatively charged polyions. Right panels: reentrant condensation (aggregate size  $R$ ) (A) and charge inversion ( $\zeta$ -potential) (B) of negatively charged hybrid niosomes, in the presence of positively charged polyions. The data are shown as a function of the charge molar ratio  $\xi$  normalized to the value  $\xi_0$  at which the measured  $\zeta$ -potential goes to zero.  $\xi$  is defined as the polyion to the lipid molar ratio. The experimental values (hydrodynamic radius measured by means of dynamic light scattering and  $\zeta$ -potential measured by means of Doppler laser electrophoretic techniques) refer to different colloidal systems. Positive charged particles: ( $\nabla$ ): DOTAP liposomes (0.8 mg/ml) and polyacrylate sodium salt; ( $\star$ ): DOTAP liposomes (1.7 mg/ml) and polyacrylate sodium salt<sup>10</sup>. Negative charge particles: ( $\circ$ ): hybrid niosomes and  $\alpha$ -polylysine; ( $\Delta$ ): hybrid niosomes and  $\epsilon$ -polylysine; ( $\square$ ): hybrid niosomes and PEVP (ionization degree 65%); ( $\diamond$ ): hybrid niosomes and PEVP (ionization degree 95%)<sup>11</sup>. Hybrid niosomes are built up by Tween20, Cholesterol and dicetylphosphate and the cationic polyion PEVP is Poly[N-ethyl-4-vinyl pyridinium] bromide.

charged surfaces. The resulting spherically symmetric potential depends on the values of the average surface potential (here assumed equal to the  $\zeta$ -potential) and on the standard deviation  $\sigma$  of the surface potential among different regions on the particle surface. In particular, Velegol and Thwar<sup>15</sup> showed that the value of the second moment of the charge distribution lowers the electrostatic repulsion.

In this work, by means of MC simulation, we analyze the aggregation process of spherical charged particles interacting via the Velegol and Thwar<sup>15</sup> DLVO-like potential. Starting from isolated monomers, we follow the growth of the aggregates until a kinetically arrested state

is reached. We study the final size of the aggregates for several values of the  $\zeta$ -potential and its standard deviation  $\sigma$ . The results of the simulations confirm that the final size of the aggregates grows on increasing  $\sigma$  and on decreasing  $\zeta$ , providing a microscopic interpretation of the re-entrant condensation phenomenon of polyion-induced charged colloidal particle aggregation (Fig. 1).

## 2. THEORETICAL BACKGROUND

According to the HHF model, the electrostatic potential of mean force  $\Phi$  between two dielectric colloidal spherical particles of radius  $R_A$  and  $R_B$  and surface potentials  $\psi_A$  and  $\psi_B$ , respectively, is given by

$$\Phi = \frac{\epsilon\pi R_A R_B}{R_A + R_B} \left[ (\psi_A^2 + \psi_B^2) \ln(1 - e^{-2\kappa H}) + 2\psi_A \psi_B \ln\left(\coth \frac{\kappa H}{2}\right) \right] \quad (1)$$

Here,  $\epsilon$  is the dielectric permittivity of dispersing medium,  $\kappa^{-1}$  is the Debye screening length and  $H$  is the minimal distance between the two particle surfaces (see fig. 2).

Eq. (1), which is derived under the conditions  $\kappa R_\alpha \gg 1$

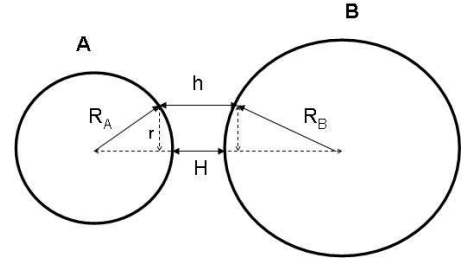


FIG. 2: Variables involved in the Derjaguin approximation, for two approaching particles of radius  $R_A$  and  $R_B$ , respectively

and  $H/R_\alpha \ll 1$  ( $\alpha=A,B$ ), holds under the following assumption: *i*)  $\psi_A$  and  $\psi_B$  are relatively small (less than 25 mV at room temperature); *ii*) the particles share the same chemical nature and are charged by similar mechanism; *iii*) the Derjaguin approximation holds<sup>12</sup>.

Velegol and Thwar<sup>15</sup> assume that the surface of a particle  $\alpha$  is partitioned in  $N$  regions (labelled by  $i$ , with  $i = 1, \dots, N_\alpha$ ) of area  $S$ , each of them characterized by a different value of the surface potential  $\psi_\alpha^i$ . These regions must be of sufficient size  $L \sim \sqrt{S}$ , so that lateral interactions can be considered negligible (practically this means that  $L \gg \kappa^{-1}$  and  $L \ll H$ ). The surface potentials  $\psi_A$  and  $\psi_B$  of two approaching particles in the HHF theory are thus replaced by the random value of the potential  $\psi_A^i$  and  $\psi_B^j$ , where  $i$  and  $j$  label the two domains (on opposite particles) facing each other. Defining  $\zeta_\alpha$  as the

average potential, one can write  $\psi_\alpha^i \equiv \zeta_\alpha + \delta_\alpha^i$  where  $\delta_\alpha^i$  a random contribution that varies among the different regions. The  $\delta_\alpha^i$  are independently distributed and not correlated, i.e.

$$\langle \psi_\alpha^i \psi_\beta^j \rangle = \begin{cases} \zeta_A^2 + \sigma_A^2 \delta^{ij}, & \text{if } \alpha = \beta = A \\ \zeta_A \zeta_B, & \text{if } A \neq B \\ \zeta_B^2 + \sigma_B^2 \delta^{ij}, & \text{if } \alpha = \beta = B \end{cases} \quad (2)$$

where  $\delta^{ij}$  is the Kröenecker delta function and  $\sigma_\alpha$  the standard deviation of surface potential on spheres of type  $\alpha$ .

The expression for the resulting potential of mean force provided by Velegol and Thwar<sup>15</sup> is

$$\Phi = \frac{\epsilon\kappa}{2} \sum_{i=1}^M \{ (\zeta_A^2 + \zeta_B^2 + 2\zeta_A \delta_i^A + 2\zeta_B \delta_i^B + \delta_A^2 + \delta_B^2) (1 - \coth \kappa h_i) + \frac{2(\zeta_A + \delta_i^A)(\zeta_B + \delta_i^B)}{\cosh \kappa h_i} \} S \quad (3)$$

where the sum runs over the  $M$  facing regions and  $h_i$  is the gap between  $i$ th regions. The ensemble averaging gives:

$$\langle \Phi \rangle = \frac{\epsilon\kappa}{2} \sum_{i=1}^M \{ (\zeta_A^2 + \zeta_B^2 + \sigma_A^2 + \sigma_B^2) (1 - \coth \kappa h_i) + \frac{2\zeta_A \zeta_B}{\cosh \kappa h_i} \} S \quad (4)$$

In order to evaluate the sum in Eq. (4), the Derjaguin approximation is applied (Fig. 2), i.e.

$$h \approx H + \frac{R_A + R_B}{2R_A R_B} r^2 \quad (5)$$

and, for any function  $F(h)$ , the following expression are employed

$$\sum_{i=1}^M F(h_i) A_i \approx 2\pi \frac{R_A R_B}{R_A + R_B} \int_0^{+\infty} F(h) dh \quad (6)$$

where  $r$  is the flat ring radius (see Fig. 2).

The resulting mean force pair interaction potential is given by

$$\langle \Phi \rangle = \frac{\epsilon\pi R_A R_B}{R_A + R_B} [ (\zeta_A^2 + \zeta_B^2 + \sigma_A^2 + \sigma_B^2) \ln(1 - e^{-2\kappa H}) + 2\zeta_A \zeta_B \ln \left( \coth \frac{\kappa H}{2} \right) ] \quad (7)$$

The mean force potential for typical values of the  $\zeta$ -potential and standard deviation  $\sigma$  is shown in Figs. 3 and 4. The potential combines a repulsive net charge-dependent monopole term ( $\zeta_\alpha \neq 0$ ) and an attractive multipole term ( $\sigma_\alpha \neq 0$ ) arising from the presence of random charge heterogeneity on the particle surface.

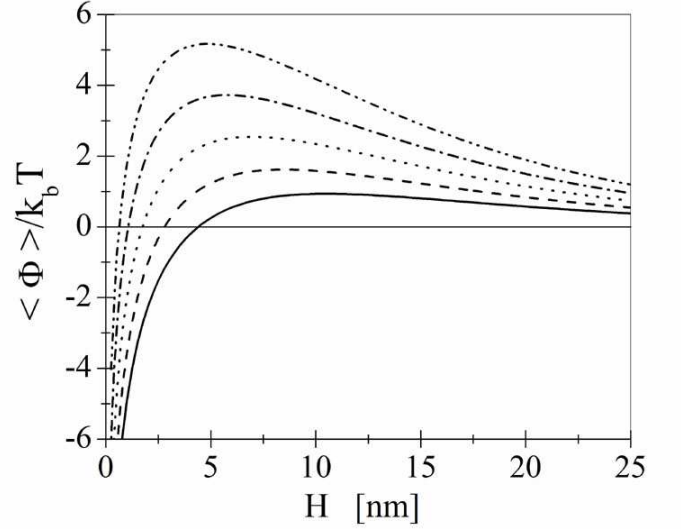


FIG. 3: Mean force potential profiles between two identical spheres calculated from Eq. (7) for different values of  $\zeta_A = \zeta_B = \zeta$  (from 11 to 19 mV) and for a constant value of  $\sigma_A = \sigma_B = \sigma = 15$  mV. Curves are plotted in units of the thermal energy  $k_b T$  at room temperature for  $R_A = R_B = R = 40$  nm and  $\kappa^{-1} = 10$  nm. Solid line:  $\zeta = 11$  mV; dashed line:  $\zeta = 13$  mV; dotted line:  $\zeta = 15$  mV; dot-dashed line:  $\zeta = 17$  mV; dot-dot-dashed line:  $\zeta = 19$  mV.

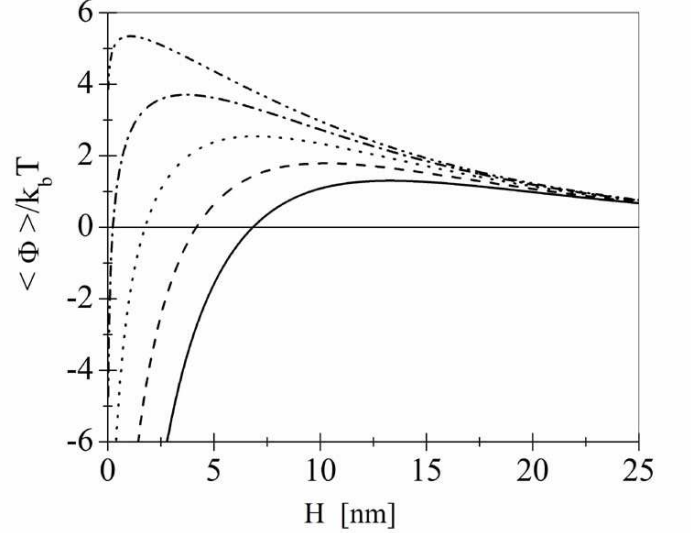


FIG. 4: Mean force potential profiles between two identical spheres calculated from Eq. (7) for different values of  $\sigma_A = \sigma_B = \sigma$  (from 5 to 25 mV) and for a constant value of  $\zeta_A = \zeta_B = \zeta = 15$  mV. Curves are plotted in units of the thermal energy  $k_b T$  at room temperature for  $R_A = R_B = R = 40$  nm and  $\kappa^{-1} = 10$  nm. Solid line:  $\sigma = 25$  mV; dashed line:  $\sigma = 20$  mV; dotted line:  $\sigma = 15$  mV; dot-dashed line:  $\sigma = 10$  mV; dot-dot-dashed line:  $\sigma = 5$  mV.

These two components lead up to a global maximum and to the presence of a potential barrier. In the case of particles with the same net charge, an attractive component is always present since the first term in Eq. (7) is negative. If the two identical particles are uniformly charged ( $\sigma_\alpha = 0$ ), both the attractive component and the global maximum vanish, recovering the HHF expression for two identical spheres (Eq. 1).

The height of the potential barrier that two approaching particles must overcome in order to aggregate and the distance between the particle surface at which this maximum occurs can be evaluated from Eq. (7). For two identical particles ( $R_A = R_B = R$ ) we obtain:

$$\langle \Phi \rangle_{max} = \pi \epsilon R \left\{ (\zeta^2 + \sigma^2) \ln \left[ 1 - \left( \frac{\zeta^2}{\zeta^2 + \sigma^2} \right)^2 \right] + \zeta^2 \ln \left[ \frac{2\zeta^2 + \sigma^2}{\sigma^2} \right] \right\} \quad (8)$$

and

$$H_{max} = \frac{1}{\kappa} \ln \left( \frac{\zeta^2 + \sigma^2}{\zeta^2} \right) \quad (9)$$

We point out that: *i*) the height of potential barrier does not depend on Debye screening length  $\kappa^{-1}$ . Consequently, addition of simple salt in bulk phase (varying the ionic strength of the solvent) does not change the strength of the interaction but only modifies the distance at which this maximum interaction occurs; *ii*) using Derjaguin approximation, a linear dependence of the barrier height on the radius  $R$  of the particles arises, underlying that larger particles interact more intensely than smaller ones and thus aggregation in the presence of large clusters is relatively inhibited; *iii*)  $\langle \Phi \rangle_{max}$  is zero when  $\zeta = 0$  and  $\lim_{\sigma \rightarrow 0+} H_{max} = 0$ , that is consistent with the statement that there is no attractive component for uniformly charged particles and that a lower value of  $\sigma$  determines a short-ranged attractive interaction.

In the framework of the above stated model, the aggregation process can be viewed as a thermally activated process strictly linked to electrostatic parameters (the  $\zeta$ -potential and its standard deviation  $\sigma$ ) and to the clusters dimensions. Colloidal particles with smaller curvature radius, lower  $\zeta$ -potential or higher charge anisotropy will be characterized by a faster aggregation dynamics. The aggregation process will slow down due to the progressive increase of the repulsive barrier on increasing the size of the aggregates.

In the next section, we introduce a MC simulation method to analyze the aggregation dynamics of spherical clusters and to evaluate the evolution of the mean cluster radius for several values of  $\zeta$ -potential and standard deviation  $\sigma$ , chosen to model the corresponding experimental range of values observed for polyion-induced liposome cluster aggregation.

In our calculations, the contribution to the attraction associated to the van der Waals interaction between two approaching particles is neglected. The reason why such interaction can be safely neglected arises from the typical range associated to the van der Waals interaction, which dyes off before  $H_{max}$ . Indeed, for liposome particles (aqueous cores of radii  $R_1$  and  $R_2$ , respectively, covered by phospholipid shell of thickness  $d$ ), the van der Waals interaction  $V_{vdW}$  can be written as<sup>17</sup>

$$V_{vdW} = -\frac{AR_1R_2}{6(R_1+R_2)} \left[ \frac{1}{H+2d} - \frac{2}{H+d} + \frac{1}{H} \right] - \frac{A}{6} \ln \left[ \frac{H(H+2d)}{2(H+d)} \right] \quad (10)$$

(where  $A$  is the Hamaker constant). For typical values of the parameters involved, eq. 10 results in a range of attraction which becomes negligible beyond  $1 \div 2$  nm. As can be seen from Figs. 3 and 4, this distance is always smaller than  $H_{max}$ . Consequently, we neglect the van der Waals interaction in the irreversible aggregation process.

### 3. SIMULATION

We study a system composed by  $N_p = 10000$  colloidal particles of initial diameter  $2R = 80$  nm in a cubic box of volume  $V$  with packing fraction  $\phi = 4\pi\rho R^3/3 = 0.01$  where  $\rho = N_p/V$  is the number density. We carry out MC simulation using local metropolis algorithm at  $T = 298$  K. Particles interact via a short range potential defined by Eq. (7). We study five different pairs of  $\zeta$  and  $\sigma$  values, comparable to typical values measured in liposome solutions<sup>10,11</sup>. We choose  $1/\kappa = 10$  nm. We recall that the value of screening length does not modify the barrier height.

Because of the compactness of the formed clusters, aggregation is modeled as an "oil drop-like process" in which the shape of the aggregates retains a spherical form. More precisely, when two approaching particles ( $A$  and  $B$ ) overcome the potential barrier (surface gap distance  $H < H_{max}$ ), they aggregate forming an unique particle with radius  $R = (R_A^3 + R_B^3)^{1/3}$  and positioned in the center of mass of two aggregating spheres. We also assume that  $S$  (the size of the uniform potential regions on the particle surface in the Velegol-Thwar expression) is independent of the cluster size. To incorporate a Brownian dynamics, in the MC algorithm, the  $i$ th particle is selected with a probability proportional to  $R_0/R_i$ , where  $R_0$  is the initial radius and  $R_i$  is the radius of the  $i$ -th aggregate<sup>18,19,20</sup>. Each selected aggregate is moved in each direction by a random quantity uniformly distributed between  $\pm 0.2$  nm. Simulations have been carried out by varying both the  $\zeta$ -potential and the variance  $\sigma^2$ . The  $\zeta$ -potential values have been chosen similar to the typical ones measured in different colloidal systems (see Fig. 1 and Refs. 10-11). On the contrary, values for

$\sigma^2$ , in absence of any experimental indication, have been chosen arbitrarily, within the validity of the model and in any case within a range of reasonable values. The aggregation process progressively slows down and simulations are interrupted when a plateau in the time dependence of the aggregate average radius or mass is reached.

#### 4. RESULTS AND DISCUSSION

In Figs. 6 and 5, we present results of the aggregation process investigated for different values of the characteristic parameters ( $\zeta$ -potential and standard deviation  $\sigma$ ).

First, we will discuss the time evolution of mean cluster radius at constant  $\sigma$  on varying the  $\zeta$ -potential. Fig. 6 shows that on increasing of the  $\zeta$ -potential, the aggregation process slows down and that the aggregates reach at long time a final limiting size. The slowing down of the dynamics is already seen at the early stage of the aggregation process, as shown in the inset of Fig. 6, consistent with the effect of  $\zeta$ -potential on the height of the potential barrier.

Fig. 5 shows the complementary case, i.e, the effect of the different values of the standard deviation  $\sigma$  at a constant value of the  $\zeta$ -potential. Again, data confirm that the increase of the random fluctuations of the charges on the particle surface speeds up the aggregation process. In all the cases investigated, the growth process slows down at long times and the aggregates appear to reach a long-time limit value, providing a strong evidence for a dynamics slow down and an arrest on the timescale sampled by our simulation. This finding suggests that a kinetically arrested state can be generated in this class of systems by the coupling between the aggregates size and the electrostatic barrier. An estimate of the characteristic size reached by the aggregates at long time can be calculated assuming that the arrest is observed on the explored time scales when the interaction energy barrier reaches an *ad-hoc* value. Indeed, inverting Eq. 8, the relation connecting the radius of interacting aggregates and the potential barrier is easily obtained. We find that, in all the cases investigated, for all the couples of  $\zeta$ -potential and standard deviation  $\sigma$  we have considered, the plateau of the average aggregate size corresponds to a characteristic barrier  $\langle \Phi \rangle_{max}$  of the order of about  $10 k_b T$  (see Figs. 6 and 5, where the normalized size  $\langle R \rangle / R_0 - 1$  calculated from eq. 8 for different values of the  $\zeta$ -potential at fixed  $\sigma$  or conversely, for different values of  $\sigma$  at fixed  $\zeta$ -potential is shown).

It is worth nothing that  $\zeta$  and  $\sigma$  values are considered to be both constant during the aggregation process that evolves from the single polyion-decorated liposome to liposome cluster. This assumption is justified as a consequence of the local character of the interaction, where only a local charge (potential) distribution determines the repulsive and attractive components of the pair potential. The distribution of the local charge of the ele-

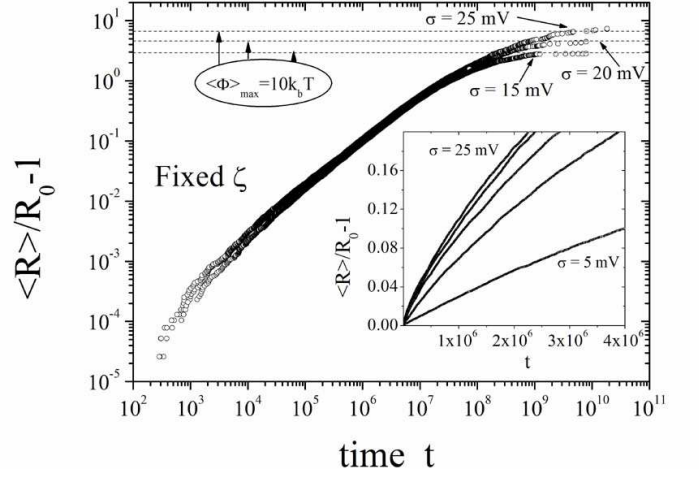


FIG. 5: Some typical time evolution of normalized mean cluster radius  $\langle R \rangle / R_0 - 1$ . Simulations have been carried out for different values of the standard deviation  $\sigma$  (in the range from 5 to 25 mV) with a constant value of the  $\zeta$ -potential  $\zeta = 15$  mV. The inset shows, in linear scale, the evolution at short times of the mean size of the aggregates, for different values of the standard deviation  $\sigma$  ( $\sigma = 25, 20, 15, 10, 5$  mV, from top to bottom, respectively).

mentary unit (single liposome) surfaces can be considered independent of the size of clusters.

In all the simulations, at short time below the slow down, the average size of clusters increases according to a power law  $\langle R \rangle / R_0 - 1 \sim at^b$  with a pre-factor that decreases from  $a = 7.2 \cdot 10^{-6}$  to  $a = 1.6 \cdot 10^{-7}$ . At the same time, the exponent  $b$  increases from  $b = 0.70$  to  $0.88$ , as the  $\zeta$ -potential varies from  $\zeta = 11$  mV to  $\zeta = 19$  mV at a constant value of  $\sigma = 15$  mV. The same behavior characterizes the  $\sigma$  dependence at fixed  $\zeta = 15$  mV in the range from  $\sigma = 25$  mV down to  $\sigma = 5$  mV. As expected, the aggregation process does not follow the diffusion limited cluster aggregation (DLCA model<sup>21</sup>) due to the presence of significant potential barriers controlling the rate of aggregation. Deviation from DLCA is also evidenced by the not negligible potential barrier height at which the arrested state occurs (of order of  $10 k_b T$ ).

Fig. 7 shows the cluster mass distributions at different stages, during the aggregation process for the case of the couple of parameters  $\zeta = 15$  mV and  $\sigma = 15$  mV. The system evolves from the initial mono-disperse distribution toward a broader distribution characterized by a well defined peak, whose position increases with time. The distribution freezes when the system kinetically arrests. The inset in Fig. 7 shows the same distribution in a semi-log scale to highlight the presence of a distribution tail compatible with an exponential distribution. Similar behavior is observed for all the cases investigated. The main differences concern the shape of the distributions in the arrested states, some of which shown in Fig. 8 (see also Table I). The final size distribution has a

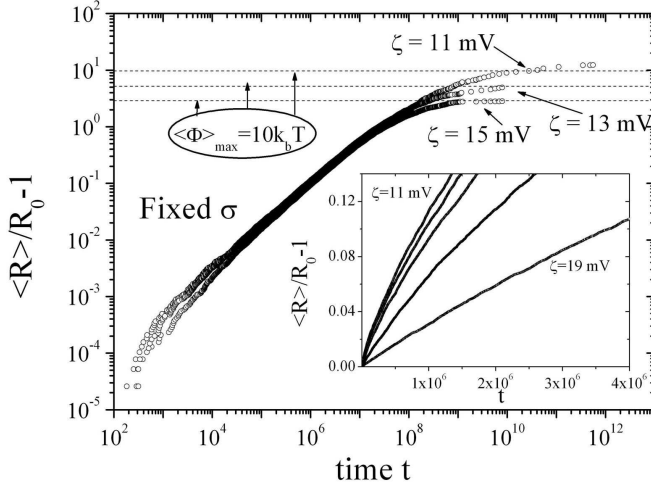


FIG. 6: Some typical time evolution of normalized mean cluster radius  $\langle R \rangle / R_0 - 1$ . Simulations have been carried out for different values of  $\zeta$ -potential (in the range from 11 to 19 mV) with a constant value of the standard deviation  $\sigma = 15$  mV. The inset shows, in a linear scale, the evolution at short times of the mean size of the aggregates for different values of the  $\zeta$ -potential ( $\zeta = 11, 13, 15, 17, 19$  mV, from top to bottom, respectively).

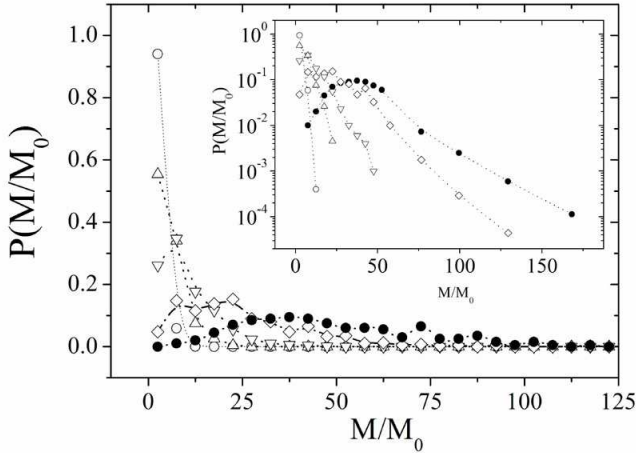


FIG. 7: Cluster size distribution of the mass  $M$  of the aggregating particles normalized to the mass  $M_0$  of the initial particles at different aggregation states for  $\zeta = 15$  mV and  $\sigma = 15$  mV. ( $\circ$ ):  $\langle M \rangle / M_0 = 2$ ; ( $\triangle$ ):  $\langle M \rangle / M_0 = 5$ ; ( $\nabla$ ):  $\langle M \rangle / M_0 = 10$ ; ( $\diamond$ ):  $\langle M \rangle / M_0 = 25$ ; ( $\bullet$ ):  $\langle M \rangle / M_0 = 50$ . Inset: the same distributions in a semi-log scale.

smaller standard deviation  $\sigma_M$  in the case of higher values of the  $\zeta$ -potential or lower values of  $\sigma$ . The average mass instead shows an opposite trend, i.e., it increases for smaller values of the  $\zeta$ -potential or higher values of  $\sigma$ .

A possible explanation of the influence of the electro-

$\zeta$ [mV]	$\sigma$ [mV]	$\sigma_M$
11	15	45.3
13	15	38.7
15	15	25.9
15	20	34.4
15	25	39.9

TABLE I: Standard deviation  $\sigma_M$  of mass distributions when  $\langle M \rangle / M_0 = 50$  for the different electrostatic parameters ( $\zeta$ -potential and its standard deviation  $\sigma$ ) used in simulations.

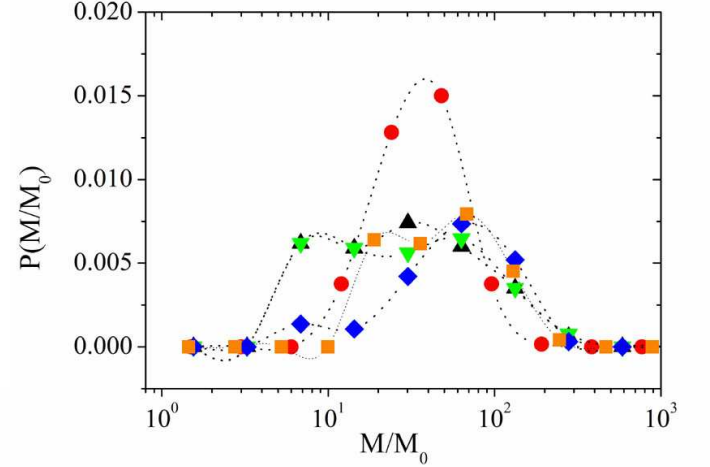


FIG. 8: (Color on line) Cluster mass distribution in a log-scale for the cluster distributions closest to the arrested state; ( $\bullet$ ):  $\zeta = 11$  mV,  $\sigma = 15$  mV; ( $\blacktriangle$ ):  $\zeta = 15$  mV,  $\sigma = 15$  mV; ( $\blacktriangledown$ ):  $\zeta = 15$  mV,  $\sigma = 25$  mV; ( $\blacklozenge$ ):  $\zeta = 15$  mV,  $\sigma = 20$  mV; ( $\blacksquare$ ):  $\zeta = 13$  mV,  $\sigma = 15$  mV.

static parameters,  $\zeta$ -potential and standard deviation  $\sigma$ , on the variance  $\sigma_M$  of the cluster size distribution is provided in Fig. 9. Here, we compare the potential profiles (eq. 7) where a particle interacts with particles of different sizes, for two different values of the  $\zeta$ -potential (11 and 15 mV, respectively). The results show that there is a preferential aggregation which favors the increase of smaller cluster rather than the cluster of larger size. Indeed, the inter-particle potential (Eq. (7)) predicts that the test particle (particle of mass  $10M_0$  in the example sketched in Fig. 9) preferentially interact with clusters of smaller size (particle of mass  $50M_0$ ) rather than with clusters of larger size (particle of mass  $200M_0$ ). This kind of preferential interaction, which becomes relatively more and more favorable for larger values of  $\zeta$ , favors the aggregation of the smaller clusters in the system. These privileged interactions result in the formation of aggregate size distributions whose width decreases with increasing  $\zeta$  or decreasing  $\sigma$ , as shown in Fig. 8.



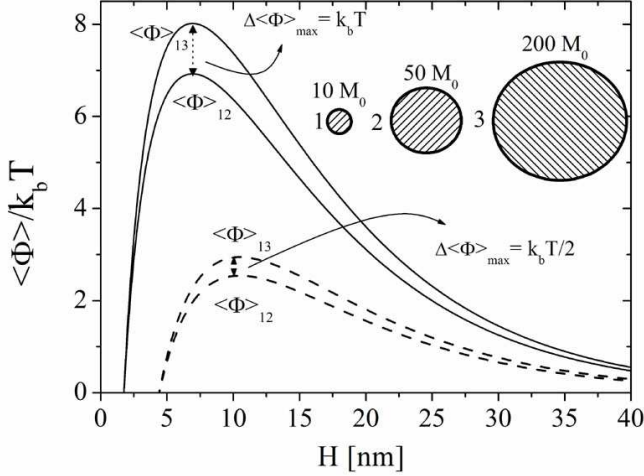


FIG. 9: The influence of the particle size on the interaction potential  $\langle\Phi\rangle$ . The graph shows the case of a particle "1" (with mass  $10M_0$ ) interacting with particle "2" (with mass  $50M_0$ ) and particle "3" (with mass  $200M_0$ ), respectively, for two different values of the  $\zeta$ -potential:  $\zeta=11$  mV (dashed lines),  $\zeta=15$  mV (full lines). As can be seen, particle "1" preferentially aggregates with particle "2" rather than with particle "3", to which corresponds a higher potential barrier.

## 5. COMPARISON WITH THE EXPERIMENTAL DATA

Eq. 8 provides a connection between the experimentally measured values of the radius  $R$  and the  $\zeta$ -potential of the cluster aggregates and the unknown value of the variance  $\sigma^2$  of the surface potential  $\psi$ . This quantity can be evaluated for the different systems shown in Fig. 1, i.e., cationic particles in the presence of anionic polyions and, conversely, anionic particles in the presence of cationic polyions. Fig. 10 shows the dependence of the standard deviation  $\sigma$  normalized to the value of the  $\zeta$ -potential,  $|\sigma/\zeta|$ , as a function of the normalized molar charge ratio  $\xi/\xi_0$ . Here,  $\xi$  is defined as the ratio between the polyion and lipid molar concentrations and  $\xi_0$  is the value of  $\xi$  at which the  $\zeta$ -potential goes to zero. As can be seen, there is a more or less pronounced decrease of  $|\sigma/\zeta|$  as a function of charge ratio  $\xi/\xi_0$  for all the systems investigated, as one can expect when more and more polyion adsorption results in a more uniform charge distribution.

A final comment is in order. Experimentally, in some of the colloidal systems investigated, it has been observed that, close to the point of charge inversion, the aggregates do not reach an equilibrium radius, but their size continues to increase with time, until, in long time limit, aggregates flocculate. This window of  $\xi/\xi_0$  values is indicated as a dashed area in Fig. 10. Interestingly, if the value of the aggregate radius measured just before flocculation is used in Eq. 8 in conjunction with the corresponding

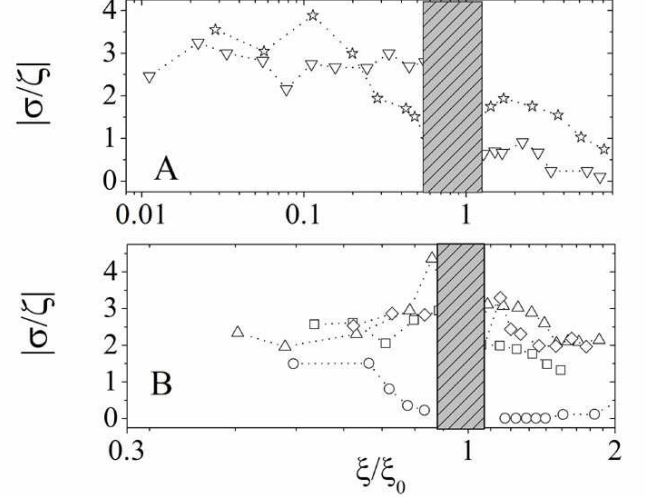


FIG. 10: The ratio  $|\sigma/\zeta|$  calculated from eq. 8 on the basis of the experimental values of radius  $R$  and the  $\zeta$ -potential of the aggregates formed in different polyion-induced particle aggregations. The marked regions correspond to the experimental instability of the aggregates, where their average size increases with time, until, in long time limit, they flocculate. A: Positive charged particles: ( $\nabla$ ): DOTAP liposomes (0.8 mg/ml) and polyacrylate sodium salt; ( $\star$ ): DOTAP liposomes (1.7 mg/ml) and polyacrylate sodium salt<sup>10</sup>. B: Negative charged particles: ( $\circ$ ): hybrid niosomes and  $\alpha$ -polylysine; ( $\triangle$ ): hybrid niosomes and  $\epsilon$ -polylysine; ( $\square$ ): hybrid niosomes and PEVP (ionization degree 65%); ( $\diamond$ ): hybrid niosomes and PEVP (ionization degree 95%)<sup>11</sup>. Hybrid niosomes are built up by Tween20, Cholesterol and dicethylphosphate and the cationic polyion PEVP is Poly[N-ethyl-4-vinyl pyridinium] bromide.

$\zeta$ -potential value, no physical solution for  $\sigma$  is recovered. More precisely, the region of  $R$  and  $\zeta$  values for which no physical solutions for  $\sigma$  exist is delimited by the curve  $\sigma = 0$ . Along this curve, the equilibrium radius depends on  $\zeta$ -potential according to

$$R = \frac{10k_b T}{\pi \epsilon \zeta^2 \ln 4} \quad (11)$$

. All the points falling in the dashed windows (instability windows) of Fig. 10 are positioned in this area of  $R - \zeta$  plane (dashed area in Fig. 11) thus we find particularly convincing the fact that the Velegol and Thwar potential provides an estimate of this unstable region because of the close agreement with the experimental results.

## 6. CONCLUSIONS

A large body of experimental<sup>1,2,10</sup>, theoretical<sup>6,7,8</sup> and simulation<sup>22</sup> investigations have shown that linear flexible or semiflexible polyions induce the aggregation of oppositely charged colloidal particles displaying a large variety of possible structures, thus emphasizing the many

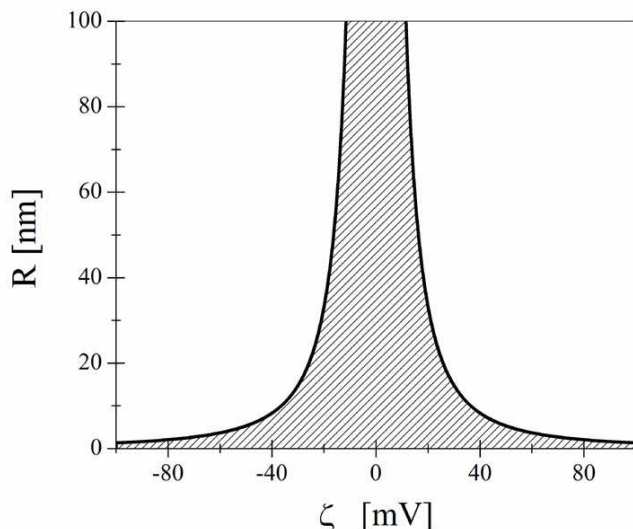


FIG. 11: Prohibited region under the curve defined by expression (11) for  $T = 298\text{ K}$  and permittivity  $\epsilon$  of water.

facets of charged macroion complex formation. Among these structures, clusters of liposomes stuck together by oppositely charged polyions form a class of model colloids in soft-matter physics which are of the great importance in many biotechnological implications. In these cases, the attractive interaction contribution to the inter-particle potential is originated by a correlated adsorption at the particle surface, which causes a non-homogeneous

charge distribution at the particle surface.

Since the major driving force of these processes is of electrostatic origin, more refined interaction potentials should be used to take into account some peculiar features in the aggregate cluster formation. We have modeled particle interactions by means of a mean force inter-particle potential recently proposed by Velegol and Thwar, who developed a closed form analytical model to estimate the effect of a non-uniform charge distribution. Within the scenario of polyion-induced charged particle aggregation, this potential provides a justification for why an attractive contribution arises in like-charged particle interactions in the presence of heterogeneities on the charged surface.

Monte Carlo simulations have been carried out for an ensemble of particles interacting via a DLVO-like-Velegol and Thwar potential, for different values of the parameters characterizing the system. Simulations qualitatively reproduce all experimentally observable trends in a variety of different colloidal systems, from positively charged liposomes in the presence of anionic polyions to negatively charged hybrid niosomes in the presence of cationic polyions. In particular, simulations clearly evidence the formation of an arrested cluster phase, which is the sign of a kinetic arrested state in low-density colloidal suspensions.

For electrostatically highly coupled systems, the use of the Velegol and Thwar potential offers an interesting promise for the understanding of the role of electrostatic attractive and repulsive interactions between charged colloidal particles and oppositely charged polyions.

- 
- <sup>1</sup> F. Bordi, C. Cametti, S. Sennato, and D. Viscomi, *J. Chem. Phys.* **126**, 024902 (2007).
  - <sup>2</sup> F. Bordi, C. Cametti, M. Diociaiuti, and S. Sennato, *Phys. Rev. E R. Comm.* **71**, 050401 (2005).
  - <sup>3</sup> D. Napper, *Polymeric Stabilization of Colloidal Dispersion* (Academic, London, 1983).
  - <sup>4</sup> J. H. Felgner, R. Kumar, C. N. Sridhar, C. J. Wheeler, Y. J. Tsai, R. Border, P. Ramsey, M. Martin, and P. L. Felgner, *J. Biol. Chem.* **269**, 2550 (1994).
  - <sup>5</sup> J. Felgner, *Proc. Natl. Acad. Sci. USA.* **84**, 7413 (1987).
  - <sup>6</sup> T. T. Nguyen and B. I. Shklovskii, *J. Chem. Phys.* **114**, 5905 (2001).
  - <sup>7</sup> T. Nguyen, A. Grosberg, and B. Shklovskii, *Phys. Rev. Lett.* **85**, 1568 (2000).
  - <sup>8</sup> A. Y. Grosberg, T. Nguyen, and B. I. Shklovskii, *Rev. Mod. Phys.* **74**, 329 (2002).
  - <sup>9</sup> M. P. D. Lima, S. Simoes, P. Pires, and H. Faneca, *Phys. Rev. E* **71**, 050401 (2005).
  - <sup>10</sup> F. Bordi, C. Cametti, S. Sennato, and D. Viscomi, *Phys. Rev. E R. Comm.* **74**, 030402R (2006).
  - <sup>11</sup> S. Sennato, F. Bordi, C. Cametti, C. Marianecchi, and M. Carafa, *J. Phys. Chem. B*, (2007, 10.1021/jp 0775449).
  - <sup>12</sup> E. J. W. Verwey and J. T. G. Overbeek, *Theory of the Stability of Lyophobic Colloids* (Elsevier, Amsterdam, 1948).
  - <sup>13</sup> S. Sennato, F. Bordi, C. Cametti, M. Diociaiuti, and P. Malaspina, *Biochem. Biophys. Acta.* **1714**, 11 (2005).
  - <sup>14</sup> J. Mou, D. Czajkowsky, Y. Zhang, and Z. Shao, *FEBS Lett.* **371**, 279 (1995).
  - <sup>15</sup> D. Velegol and P. K. Thwar, *Langmuir* **17**, 7687 (2001).
  - <sup>16</sup> R. Hogg, T. W. Healy, and D. W. Fuerstenau, *Trans. Faraday Soc.* **62**, 1638 (1966).
  - <sup>17</sup> R. Tadmor, *J. Phys. Cond. Mat.* **13**, L195 (2001).
  - <sup>18</sup> S. Babu, M. Rottureau, T. Nicolai, J. C. Gimel, and D. Durand, *Eur. Phys. J. E* **19**, 203 (2006).
  - <sup>19</sup> S. Babu, M. Rottureau, J. C. Gimel, and T. Nicolai, *J. Chem. Phys.* **125**, 184512 (2006).
  - <sup>20</sup> B. H. Zimm, *J. Chem. Phys.* **24**, 269 (1956).
  - <sup>21</sup> T. A. W. Jr and L. M. Sander, *Phys. Rev. Lett.* **19**, 1400 (1981).
  - <sup>22</sup> R. Messina, C. Holm, and K. Kremer, *Phys. Rev. E* **65**, 041805 (2002).